research article

Radiological findings of porcine liver after electrochemotherapy with bleomycin

Maja Brloznik[1], Nina Boc[2], Gregor Sersa[2,3], Jan Zmuc[2], Gorana Gasljevic[2], Alenka Seliskar[1], Rok Dezman[4], Ibrahim Edhemovic[2], Nina Milevoj[1], Tanja Plavec[1,5], Vladimira Erjavec[1], Darja Pavlin[1], Masa Bosnjak[2], Erik Brecelj[2], Ursa Lampreht Tratar[2], Bor Kos[6], Jani Izlakar[2], Marina Stukelj[7], Damijan Miklavcic[6], Maja Cemazar[2,8]

[1] University of Ljubljana, Veterinary Faculty, Small Animal Clinic, Ljubljana, Slovenia
[2] Institute of Oncology Ljubljana, Ljubljana, Slovenia
[3] University of Ljubljana, Faculty of Health Sciences, Ljubljana, Slovenia
[4] University Medical Centre, Clinical Institute of Radiology, Ljubljana, Slovenia
[5] Small Animal Hospital Hofheim, Katharina-Kemmler-Strasse 7, Hofheim, Germany
[6] University of Ljubljana, Faculty of Electrical Engineering, Ljubljana, Slovenia
[7] University of Ljubljana, Veterinary Faculty, Clinic for Reproduction and Farm Animals, Clinic for Ruminants and Pigs, Ljubljana, Slovenia
[8] University of Primorska, Faculty of Health Sciences, Izola, Slovenia

Background. Radiologic findings after electrochemotherapy of large hepatic blood vessels and healthy hepatic parenchyma have not yet been described.

Materials and methods. We performed a prospective animal model study with regulatory approval, including nine grower pigs. In each animal, four ultrasound-guided electroporated regions were created; in three regions, electrodes were inserted into the lumen of large hepatic vessels. Two types of electrodes were tested; variable linear- and fixed hexagonal-geometry electrodes. Ultrasonographic examinations were performed immediately and up to 20 minutes after the procedure. Dynamic computed tomography was performed before and at 60 to 90 minutes and one week after the procedure.

Results. Radiologic examinations of the treated areas showed intact vessel walls and patency; no hemorrhage or thrombi were noted. Ultrasonographic findings were dynamic and evolved from hyperechogenic microbubbles along electrode tracks to hypoechogenicity of treated parenchyma, diffusion of hyperechogenic microbubbles, and hypoechogenicity fading. Contrast-enhanced ultrasound showed decreased perfusion of the treated area. Dynamic computed tomography at 60 to 90 minutes after the procedure showed hypoenhancing areas. The total hypoenhancing area was smaller after treatment with fixed hexagonal electrodes than after treatment with variable linear geometry electrodes.

Conclusions. Radiologic findings of porcine liver after electrochemotherapy with bleomycin did not show clinically significant damage to the liver, even if a hazardous treatment strategy, such as large vessel intraluminal electrode insertion, was employed, and thus further support safety and clinical use of electrochemotherapy for treatment of hepatic neoplasia.

Key words: electrochemotherapy; pig; liver; hepatic vessels; ultrasound; computed tomography

Introduction

Surgical resection is the gold standard for the treatment of hepatic neoplasia. However, the majority of hepatic tumors are unresectable at the time of diagnosis. In these patients, alongside systemic chemotherapy, different local ablative techniques, such as radiofrequency and microwave ablation, are used.[1-3] However, these two techniques are not optimal for tumors located near major bile ducts and larger hepatic vessels due to the heat sink effect or potential damage to vital structures.[2-4] Hence, novel techniques, such as irreversible electroporation (IRE) ablation and electrochemotherapy (ECT), are advantageous for patients with unresectable hepatic neoplasia adjacent to major bile ducts and vessels.[1-3,5] ECT is a method for the delivery of chemotherapeutic drugs by reversible electroporation, which enables the entry of otherwise poorly or nonpermeant exogenous molecules into cells by the application of short high-intensity electric pulses that induce reversible cell membrane permeabilization.[6-8] ECT is nowadays widely used in European centers for the treatment of cutaneous tumors.[9,10]

Clinical studies have shown that ECT is safe and effective also for the treatment of liver metastases and hepatocellular carcinoma (HCC)[3,4,6,7,11–13], and also other deep-seated tumors like pancreatic carcinoma.[14-16] Potentially hazardous electrode insertion into the lumen of major hepatic vessels has been reported in a study with percutaneous ECT of portal vein tumor thrombosis in patients with HCC.[11] From ECT[3,4,6,7,11,12] and IRE[17-22] studies, it is assumed that ECT of large hepatic vessels is safe, but this assumption has not yet been demonstrated with early radiologic examinations, which could reveal possible intra-abdominal hemorrhage or thrombus formation that could prove fatal for the patient.

Radiologic findings after IRE of hepatic tissue have been thoroughly described and used to determine the area that was irreversibly electroporated[22-26], while there has only been one report of radiologic findings after ECT of liver, where ultrasonographic (US) changes in hepatic tumors were described as indicators of adequate electric field tumor coverage for effective ECT.[27] The effect of ECT on healthy hepatic parenchyma and large hepatic vessels has not been previously studied by diagnostic imaging methods. The aim of this study was to characterize radiologic findings after ECT of large hepatic vessels and hepatic parenchyma in a porcine model, and hence to confirm the safety of the procedure.

Materials and methods

Animals and ethics approval

In this prospective animal model study with regulatory approval issued by the National Ethics Committee at The Administration of the Republic of Slovenia for Food Safety, Veterinary, and Plant Protection (Approval number: U34401-1/2017/4, Approval date: 17.03.2017), nine female grower pigs, purchased from an authorized swine breeder (Globocnik, Sencur, Slovenia) 3–17 days before experiment, were included.[28] Experimental animals were reared according to the European Council directive for minimum standards for the protection of pigs (2008/120/EC). All procedures complied with relevant national and European legislation (2010/63/EU).

Animals were 12 weeks old, weighed 31 ± 2.5 kg, and their liver volume estimated from CT images was 865 ± 85 cm^3.

Electrochemotherapy

During open surgery, four US-guided electroporated regions were created.

Insertion of electrodes. Electrodes were inserted into the lumen of the caudal vena cava and surrounding hepatic parenchyma (region 1), into the left median hepatic vein and surrounding parenchyma (region 2), into the left portal vein and parenchyma (region 3), and in the hepatic parenchyma of the left liver lobe (region 4).

Bleomycin and control group. Two pigs served as a control group and received electric pulses (EP) only. In the remaining seven pigs, ECT was performed; bleomycin (Bleomycinum, Heinrich Mack Nachf. GmbH & CO. KG, Illertissen, Germany, 15.000 IE/m^2) was administered intravenously at 8 minutes before the first application of EP.

Types of electrodes. Two types of electrodes routinely used in clinical treatment were tested. Variable linear geometry electrodes consisted of two long needle electrodes (with a diameter of 1.2 mm and a 3 cm long active part), which were 2 cm apart (VG-1230T12, IGEA S.p.A., Carpi, Italy). These electrode were employed in five cases of ECT and the two cases of EP. Fixed hexagonal geometry electrodes consists of seven needle electrodes with a diameter of 0.7 mm that are hexagonally placed 0.73 cm apart in a round plastic holder (N-30-HG, IGEA). These electrodes were used in two cases of ECT.

Electric pulses. EP was delivered with an electric pulse generator (Cliniporator, IGEA), and the

number of pulses for linear and hexagonal geometry electrodes were 8 and 96, respectively (8 between each individual electrode pair). Each pulse was 100 microseconds long, and the voltage was set to 2000 V in the case of linear electrodes and 730 V in the case of hexagonal electrodes. The frequencies for the linear and hexagonal electrode geometries were 1 and 5000 Hz, respectively.

Numerical modeling of electric field distribution

The treated area electric field was calculated by the finite element method using the software package Comsol Multiphysics (COMSOL AB, Stockholm, Sweden) with MATLAB (Mathworks, Natick, MA, USA).[29,30] The electrical parameters and bleomycin dosage were consistent with the European standard operating procedures for the ECT protocol and ECT for colorectal liver metastases clinical trials.[3,31,32]

Study end-point

The animals were euthanized at two or seven days after ECT/EP using 3 ml/10 kg i.v. T61 euthanasia solution (Intervet, Boxmeer, Netherlands); the liver was explanted for histologic analyses, which were reported in a separate paper.[28]

Ultrasonography (US) and computed tomography (CT)

Ultrasonographic examinations (US) were performed immediately and up to 20 minutes after the procedure. Different US machines were used, as available: Resona 7 and/or M9 (Mindray, Shenzhen, China) and/or Logiq S7 Pro (GE, Milwaukee, WI, USA). US examinations included B-mode to provide information about echogenicity and echotexture changes, Doppler (color and pulse-wave) to examine vessel patency and contrast enhanced ultrasound (CEUS) to evaluate the perfusion of hepatic parenchyma. The region of CEUS investigation was chosen according to the available US machine. In the case of the Mindray machine, a linear probe was used and the near-field area was preferred, whereas with the GE machine, the far-field was chosen since contrast works only with a convex probe. CEUS was performed before and after EP/ECT. Low mechanical index (<0.1) was applied, and a transpulmonary contrast agent Sonovue (Bracco, Milan, Italy), based on sulfur hexafluoride microbubbles, was administered into the cephalic vein (2.4 ml), and then flushed with saline (2 ml).

From the time of contrast application, a 90-second cine-clip was made for further image analysis.

CT of the liver was performed before and at 60 to 90 minutes after EP/ECT with a Somatom Scope CT scanner (Siemens, Erlangen, Germany) in seven pigs. In two pigs treated with ECT with variable linear geometry electrodes, CT was also performed at 1 week after ECT. The following CT parameters were used: referenced 170 mA, 110 kVp, 3.0 mm slice reconstruction thickness, 2.0 mm reconstruction increment, and beam pitch of 1.4. The dynamic study with the contrast medium iopromide (Ultravist; Bayer, Leverkusen, Germany, 0.5 ml/kg), which was administered intravenously with a Missouri dual chamber injector pump (Ulrich medical, Ulm, Germany) at a velocity of 3 ml/s, consisted of 5 phases: pre-contrast, arterial with bolus tracking in abdominal aorta, and 3 subsequent phases in 30-second intervals (at 30, 60 and 90 seconds after arterial phase).

Image analysis

All radiologic findings were interpreted in consensus by three radiologists (M.B., N.B., R.D.) with more than 10-years of experience in liver imaging.

CEUS perfusion curve, presenting the signal intensity, was analyzed with the US machine built-in software.

CT images were evaluated with a free and open source software program Horos (https://horosproject.org) and Impax 6 (Agfa HealthCare, Mortsel, Belgium). CT findings before and after EP/ECT were compared. Hepatic attenuation, contrast enhancement, vessel patency, diameter and possible extravasation were evaluated. In pre-contrast studies, hepatic attenuation has been evaluated subjectively for homogeneity of hepatic parenchyma and circular ROIs were used to measure the attenuation in Hounsfield units (HU). Vessel patency, diameter and possible extravasation were evaluated subjectively in contrast studies. Dynamic CT showed hypoenhancing areas, which were if compared to untreated areas most clearly seen at 30 or 60 seconds after arterial phase. In each animal, the phase with the most evident hypoenhancing regions was used for further evaluation. Attenuation of untreated hepatic parenchyma was measured with circular ROIs that did not include vessels. Since it was difficult to differentiate individual treatment regions, all hypoenhancing areas were measured; in each of the transverse CT images, all the hypoenhancing regions were carefully delineated (with manual ROIs) to measure the area (in mm^2) and attenuation (in

HU) of the region. The total area, mean area and attenuation of the total area were calculated for each animal. The latter was calculated by a mathematical formula *sum (area x attenuation / total area)*. To exclude individual differences in contrast enhancement, attenuation of untreated hepatic parenchyma was also considered; the difference between the attenuation of untreated parenchyma and the attenuation of the total area was divided by the attenuation of untreated parenchyma and multiplied by 100.

Histology

Histologic examinations were performed by an experienced pathologist (G.G.) with more than 10-years of experience in surgical pathology. To provide a comparison of radiologic and histologic data, immediate core biopsies of ECT-treated and untreated areas were performed in two pigs treated with ECT using linear geometry electrodes. In the treated parenchyma, two biopsies located between and oriented parallel to the electrodes were collected: one adjacent to the electrode and one 1 cm away from the electrode to the middle of the treated area. Histologic samples were fixed over-

night in 10% buffered formalin, embedded in paraffin, cut into 3- to 4-µm-thick sections and stained with hematoxylin and eosin (H&E).

Statistical analysis

Statistical package computer program SPSS (SPSS Inc., Chicago, Illinois, USA) was used. For analysis of hepatic parenchyma contrast enhancement, the Shapiro-Wilk test was utilized to test the normality. Since the variables were not normally distributed, the Mann-Whitney U test and the Kruskal Wallis H test were used. Statistical significance was defined as $P \leq 0.05$. For other data in this study, descriptive statistics were applied.

Results

Radiologic findings and numerical modeling of electric field distribution

US findings

EP were delivered only after US confirmation of electrode position (Figure 1A). Immediately after
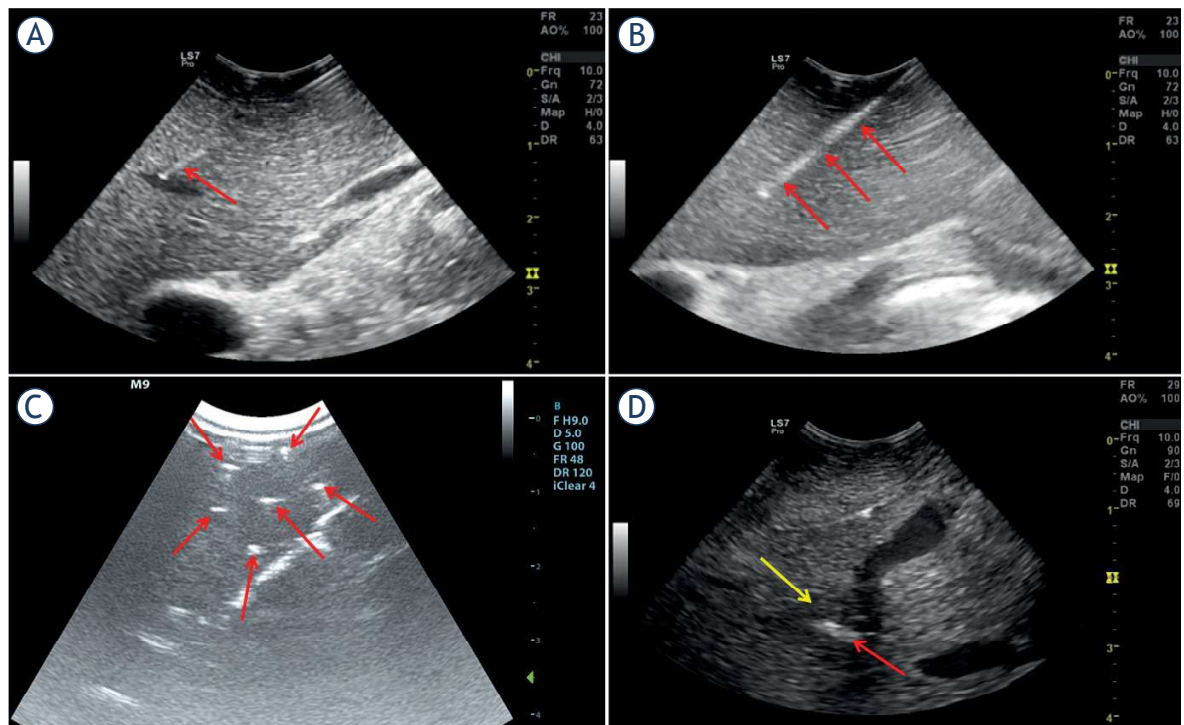

FIGURE 1. B-mode ultrasonography. **(A)** Position of the variable linear geometry electrode in the left middle hepatic vein (arrow). **(B)** Hyperechogenic microbubbles (arrows) observed immediately after electrochemotherapy (ECT) along the track of the linear electrode. **(C)** Hyperechogenic microbubbles observed immediately after ECT along the tracks of hexagonal geometry electrodes (arrows). **(D)** In the next minutes, the hepatic parenchyma of the treated area becomes hypoechogenic (yellow arrow), and hyperechogenic microbubbles (red arrow) start to diffuse.
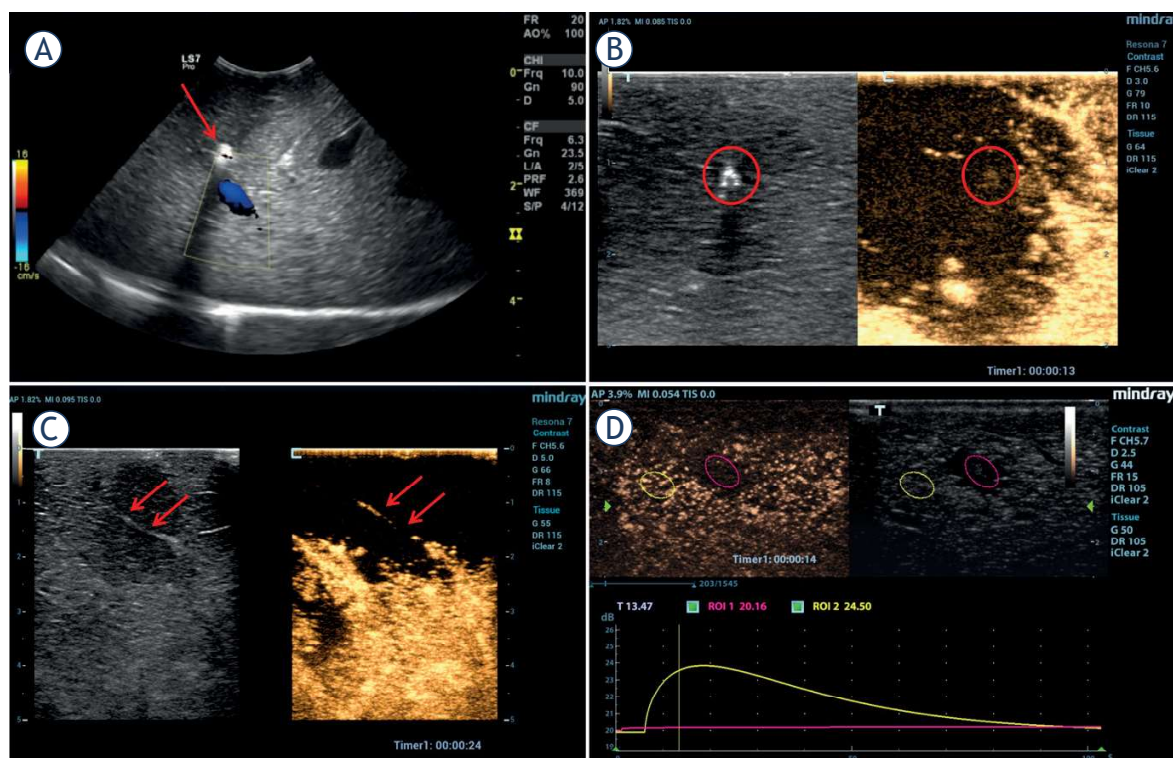
FIGURE 2. Doppler and contrast-enhanced ultrasonography. **(A)** Color Doppler in the left middle hepatic vein (blue) immediately after electrochemotherapy (ECT). Hyperechogenic microbubbles (arrow) can be noted. **(B)** Contrast enhanced ultrasound (CEUS) immediately after ECT and at 13 seconds after contrast administration; the position of the electrode is circled. **(C)** CEUS at 4 minutes after ECT and at 24 seconds after contrast; the larger vessel can be recognized (arrows). **(D)** CEUS at 5 minutes after ECT and at 14 seconds after contrast; a perfusion curve is shown.

the delivery of EP and removal of the electrodes, hyperechogenic microbubbles were observed along the electrode tracks (Figure 1B and C). In the next minutes, the treated parenchyma became hypoechogenic, and the hyperechogenic microbubbles started to diffuse (Figure 1D); the area of hypoechogenicity was larger than the area between the electrodes. In the next 5 to 10 minutes, the hyperechogenic microbubbles diffused through the treated area. There was no obvious difference between EP and ECT with variable linear geometry electrodes, while in the two cases of ECT with fixed hexagonal geometry electrodes, the hypoechogenicity was less evident compared to that with variable linear electrodes. After 10 minutes, the hypoechogenicity started to fade, and in the case of the treatment with hexagonal electrodes, it was no longer visible. The hypoechogenicity of the parenchyma was in contiguity to the treated vessel; however, the vessel wall appeared intact. There was no hemorrhage observed. Furthermore, the patency of the vessel was normal; there were no thrombi, stenotic lesions or extravasation noted, and the Doppler examination showed laminar flow (Figure 2A). CEUS showed that the perfusion of the treated area was significantly decreased (Figure 2B, C and D). The area of the hypoperfused parenchyma was larger than the area between the electrodes (Figure 2B), *i.e.* extending outside the borders of the area encompassed by the electrodes. In the case of the treatment with fixed hexagonal geometry electrodes, the decrease in perfusion was less pronounced compared to the treatment with variable linear geometry electrodes, which was consistent with computer simulation of the larger volume exposed to high strength electric fields in the variable linear geometry electrodes.

CT features

Dynamic contrast enhanced CT at 60 to 90 minutes after EP/ECT showed subtle hypoattenuating electrode tracks in the pre-contrast and arterial phases (Figure 3A and B), while in the 3 subsequent phases, hypoenhancing areas of treated hepatic parenchyma were noted (Figure 3C, D and E). These areas were most clearly observed at 30 or 60 seconds after the arterial phase, and the phase with
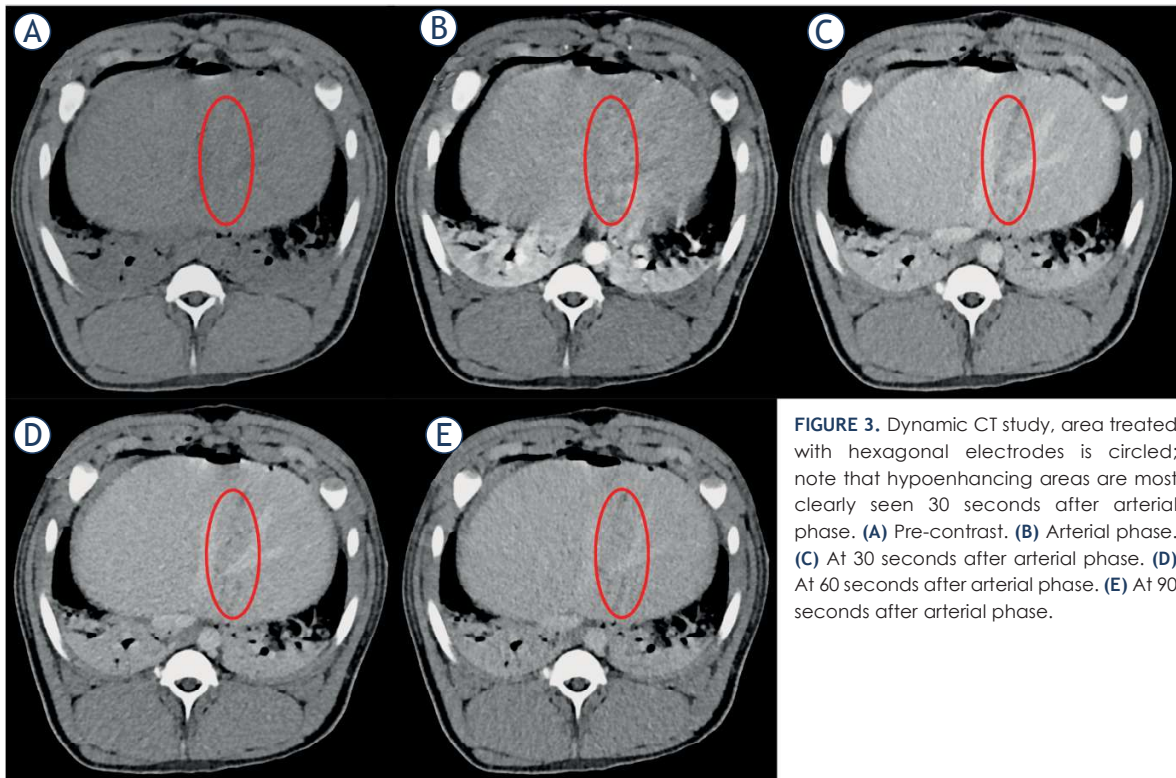
FIGURE 3. Dynamic CT study, area treated with hexagonal electrodes is circled; note that hypoenhancing areas are most clearly seen 30 seconds after arterial phase. **(A)** Pre-contrast. **(B)** Arterial phase. **(C)** At 30 seconds after arterial phase. **(D)** At 60 seconds after arterial phase. **(E)** At 90 seconds after arterial phase.

most evident hypoenhancing areas was used for further evaluation. As can be seen in Table 1, different number of hypoenhancing areas were measured in each animal. In the case of the treatment with linear geometry electrodes, the hypoenhancing regions were larger than those in the case of the treatment with hexagonal geometry electrodes (Figures 4A, B, 5A and 5B). An example of the multiplanar reconstruction (MPR) of one of the areas treated with variable linear geometry electrodes is presented in Figure 4C. All treated vessels were patent with no evidence of thrombosis (Figure 6A). Hypoenhancing areas were in contiguity with the treated vessels. There was no narrowing of the treated vessels, vessel wall and patency were not affected. No contrast extravasation was identified from large vessels in which the electrodes were inserted.

TABLE 1. Area and attenuation of hypoenhancing regions for each animal

		Number of measured hypo-enhancing regions	Total area (in mm²)	Median area (in mm²), IQR	A Attenuation of total area (in HU) ∑ ((area x attenuation) / total area)	B Attenuation of untreated parenchyma (in HU), ± SE 15 measurements in each animal	Difference in attenuation (B – A)	Corrected difference in attenuation (B–A)/B*100
Linear electrodes	ECT	48	8454	94.5, 46–168	72	118 ± 2	46	39
		66	3178	31.5, 19–53	86	114 ± 2	28	25
		91	5146	39, 25–75	82	123 ± 1	41	33
	EP	61	4538	51, 30–104	75	108 ± 1	33	30
		55	3563	32, 18–92	122	165 ± 3	43	26
Hexagonal electrodes	ECT	25	750*	21, 11.5–32*	98	124 ± 2	26	21
		46	2328*	39.5, 25–72*	80	101 ± 1	21*	21*
1 week after ECT with linear electrodes		11	99**	8, 5–11**	74	99 ± 1	24**	25**
		13	300**	19, 12–27.5**	76	101 ± 1	25**	25**

ECT = electrochemotherapy; EP = electroporation; HU = Hounsfield units; IQR = interquartile range; STD = standard deviation; *P < 0.01 compared to groups with variable linear geometry electrodes; **P < 0.01 compared to groups immediately after EP/EC
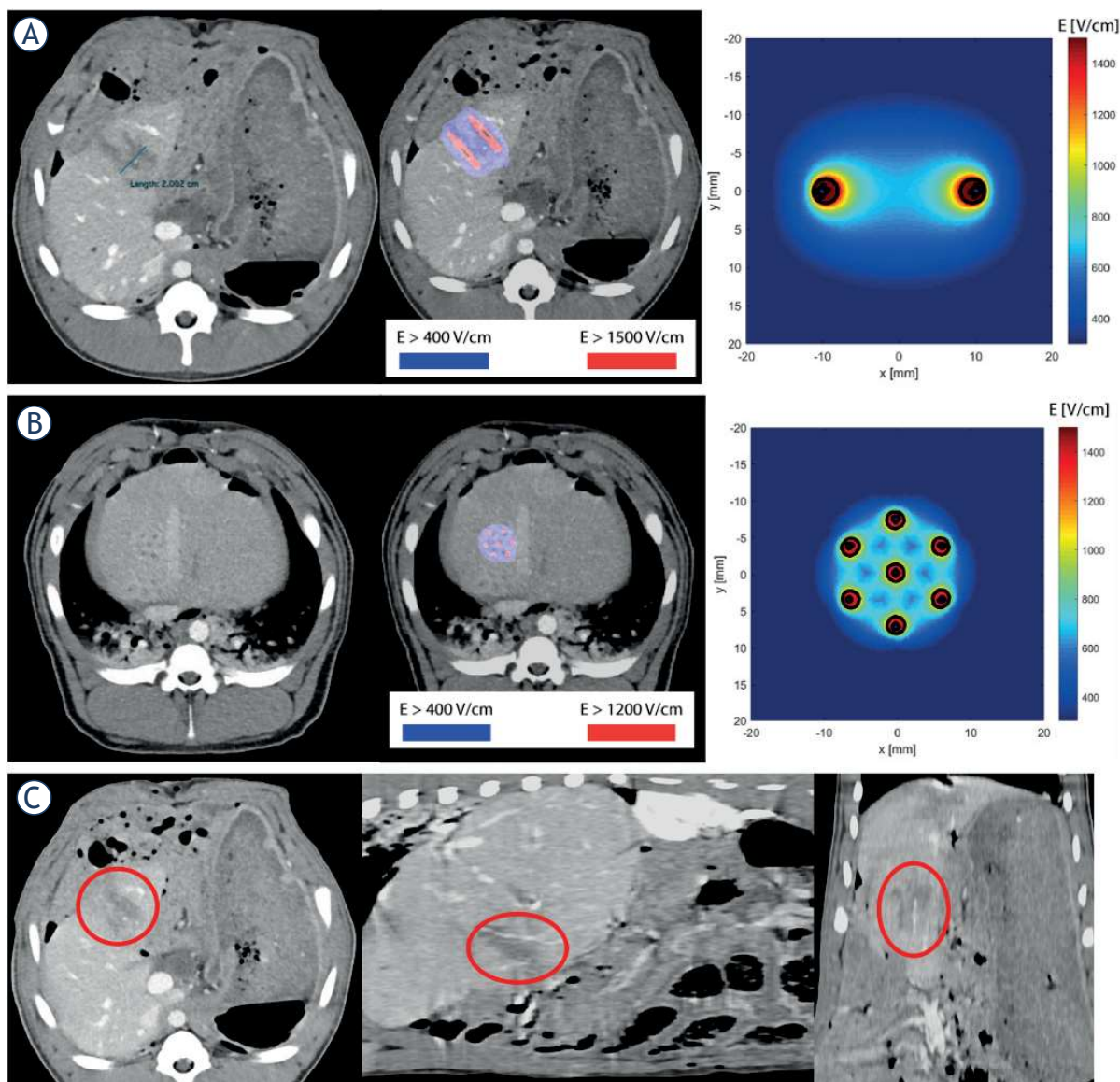
FIGURE 4. (A) Electrochemotherapy (ECT) of the liver with linear electrodes. Left figure is a CT image, where a distance between the hypoenhancing tracks of 2 cm can be noted. Right figure is numerical model of electric field distribution in linear electrodes. Middle figure shows electric field distribution superimposed on the CT image. **(B)** ECT of the liver with hexagonal electrodes. Left figure is a CT image and right figure is numerical model of electric field distribution in hexagonal electrodes. Middle image shows electric field distribution superimposed on the CT image. **(C)** Multiplanar reconstruction (MPR) of Figure 4A. The hypoenhancing area is circled. Note the larger vessel in the middle of the hypoenhancing area in coronal reconstruction.

After careful delineation of the hypoenhancing areas in each of the transverse CT images (Figure 6B), a statistically significant difference between attenuation of untreated parenchyma and attenuation of treated areas was observed in all animals. For each animal, CT measurements and calculations are presented in the Table 1. In the case of the treatment with hexagonal geometry electrodes, the total area of the hypoenhancing regions was smaller than that in the case of the treatment with linear electrodes ($P < 0.001$), which is in accordance with computer simulation. The results of the computer simulations are shown in Figure 4A and B, where the difference in the shape of the local electric field strength produced by the different electrodes is observed. Figure 4A shows that the treated volume produced by the variable linear geometry electrodes measures 30 mm in width and 20 mm in height (corresponding to the distance between the electrodes and the applied voltage) and
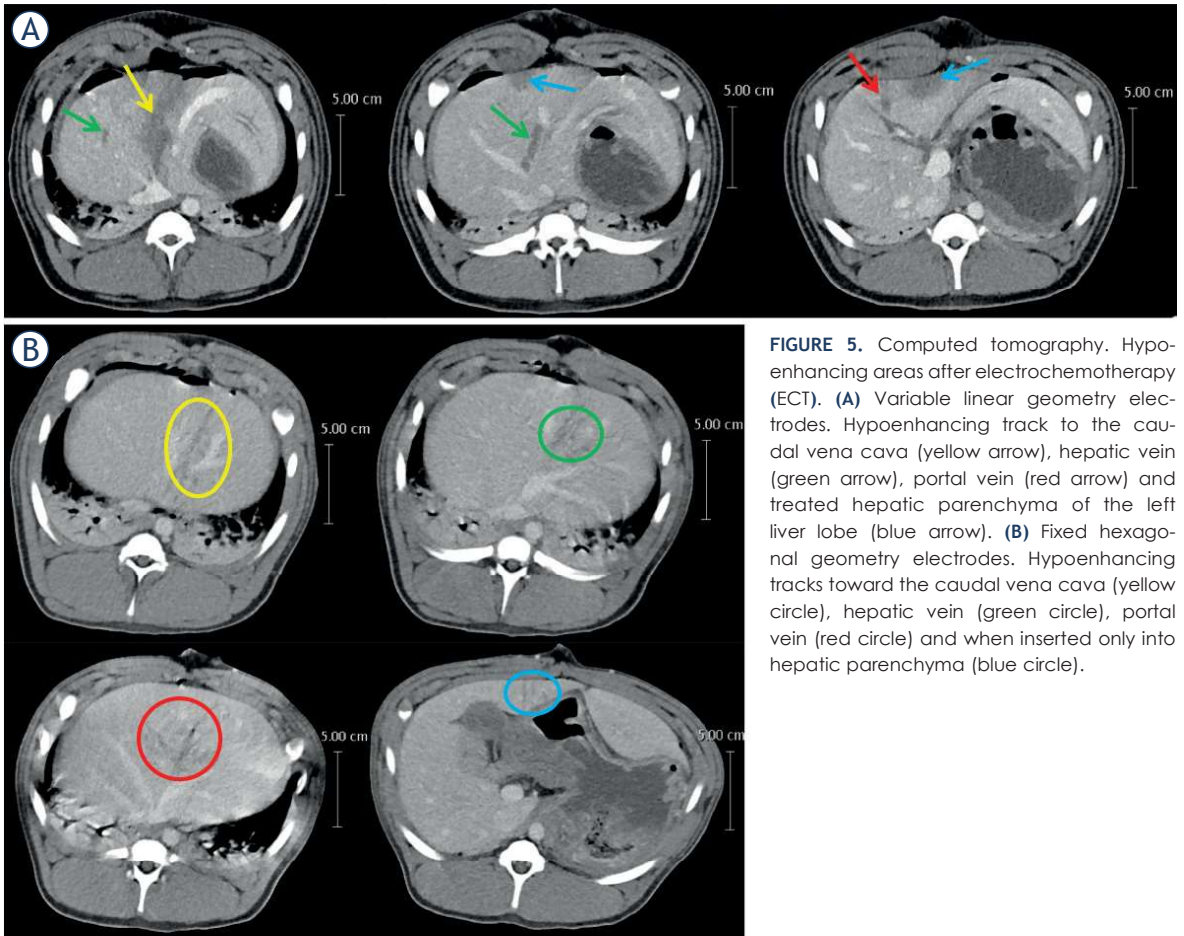
FIGURE 5. Computed tomography. Hypoenhancing areas after electrochemotherapy (ECT). **(A)** Variable linear geometry electrodes. Hypoenhancing track to the caudal vena cava (yellow arrow), hepatic vein (green arrow), portal vein (red arrow) and treated hepatic parenchyma of the left liver lobe (blue arrow). **(B)** Fixed hexagonal geometry electrodes. Hypoenhancing tracks toward the caudal vena cava (yellow circle), hepatic vein (green circle), portal vein (red circle) and when inserted only into hepatic parenchyma (blue circle).
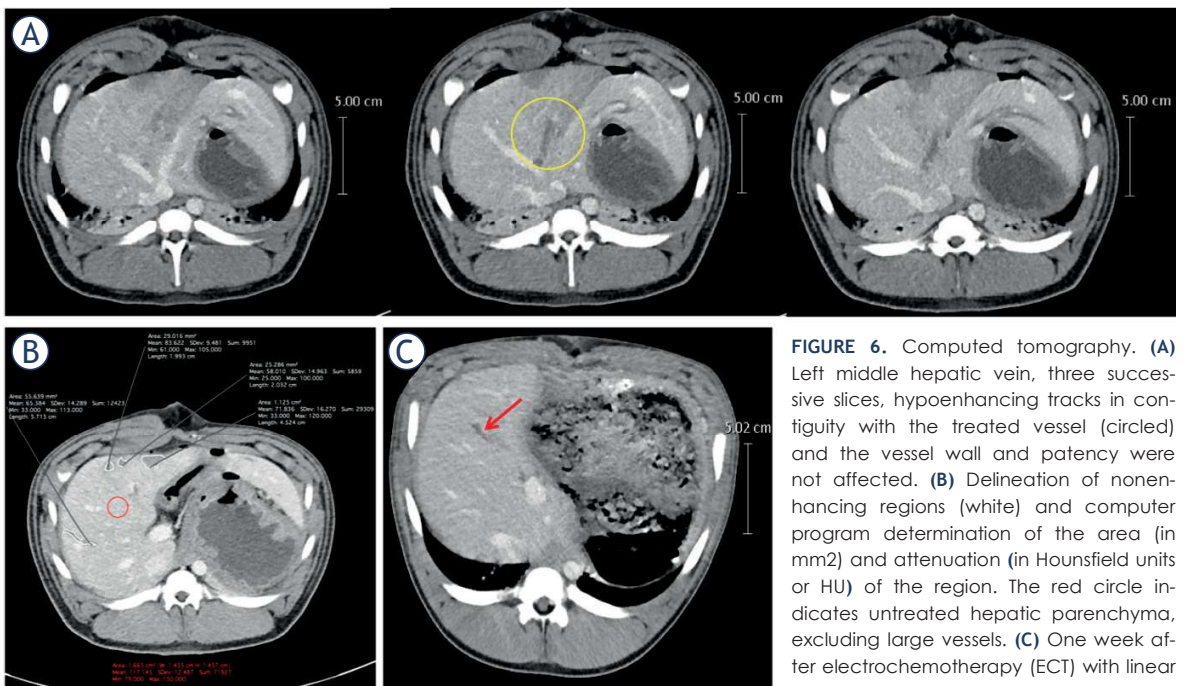

FIGURE 6. Computed tomography. **(A)** Left middle hepatic vein, three successive slices, hypoenhancing tracks in contiguity with the treated vessel (circled) and the vessel wall and patency were not affected. **(B)** Delineation of nonenhancing regions (white) and computer program determination of the area (in mm2) and attenuation (in Hounsfield units or HU) of the region. The red circle indicates untreated hepatic parenchyma, excluding large vessels. **(C)** One week after electrochemotherapy (ECT) with linear electrodes, narrow hypoenhancing tracks were observed (red arrow).
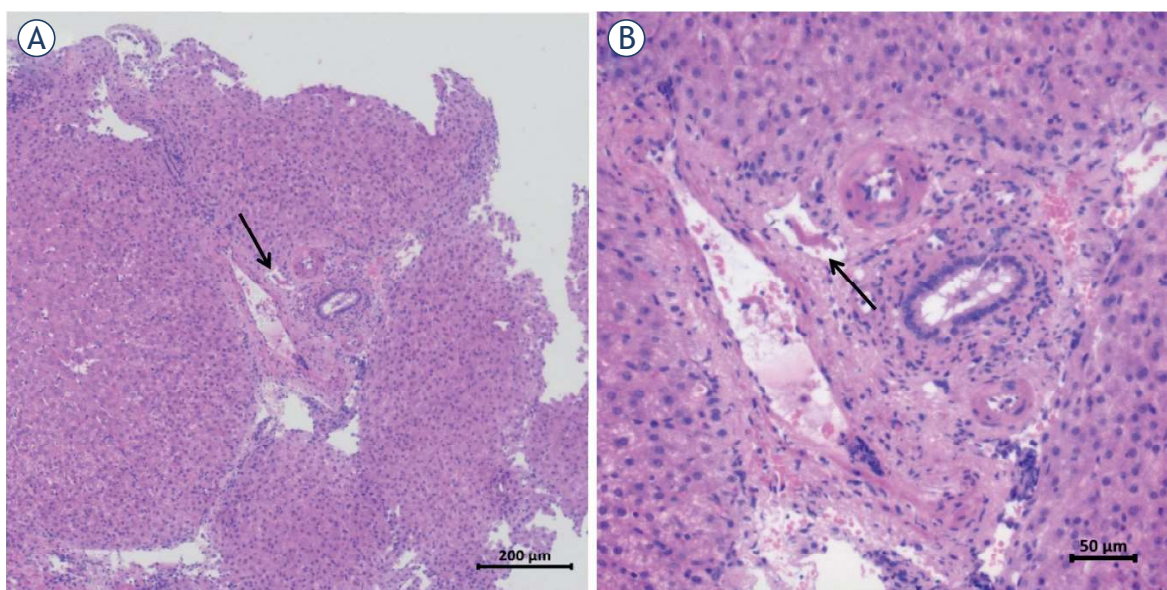
FIGURE 7. Histology of hepatic parenchyma immediately after electrochemotherapy (ECT). Fibrin thrombus in the lumen of a small venule (arrow). **(A)** H&E, 10x. **(B)** H&E, 20x.

is larger than the treated volume produced by the hexagonal electrodes, which is 20 mm by 20 mm (Figure 4B).

Furthermore, the difference and the corrected difference in attenuation were smaller after treatment with fixed hexagonal geometry electrodes than after treatment with variable linear electrodes (P < 0.001). There was no significant difference in the total area between the EP and ECT with linear electrodes (P = 0.908). In the CT findings at one week after ECT (Figure 6C), a regression of the ECT-induced changes was observed with only small hypoenhancing areas with diameters of up to 6 mm identified, which corresponds to the volume of irreversibly electroporated liver tissue determined by computer simulations, as shown in Figure 4A and B. The total area of the hypoenhancing regions was smaller than that observed immediately after the EP/ECT (P < 0.001). The difference and corrected difference in attenuation were both smaller after one week compared to those at 60 to 90 minutes after EP/ECT (P < 0.001, P = 0.007).

Histologic findings

Histologic findings of treated hepatic parenchyma immediately after ECT showed fibrin thrombi in small venules (Figure 7), with no other histologic changes of other vessels and bile ducts or the hepatic parenchyma.

Discussion

Radiologic findings after EP/ECT of large hepatic vessels and hepatic parenchyma were characterized in a porcine model, which was selected due to anatomical and physiological similarities with the human liver.[1,33] The results showed decreased perfusion in the treated area. This finding was an anticipated result since EP/ECT induces a local blood flow modifying effect or 'vascular lock' characterized by the vasoconstriction and increased wall permeabilization of small blood vessels. The effect on perfusion is shorter in EP compared to that in ECT and shorter in healthy compared to tumor tissue, which is known as the 'vascular disrupting effect'. Chemotherapeutic drugs are cytotoxic to endothelial cells, especially neoplastic endothelial cells, and this effect prolongs decreased perfusion.[34-41] In our case, there was no difference between EP and ECT, and no vascular disrupting effect was observed in healthy hepatic parenchyma[28], which confirms that bleomycin at the doses used has a negligible effect on healthy tissue.[34-36]

All radiologic modalities showed healthy vessel walls and patency, despite direct electrode insertion into the lumen of major hepatic vessels. These findings were consistent with previously published histologic results: no thrombosis was identified at two and seven days after EP/ECT in healthy liver.[28] This result was an expected finding considering

ECT[3,4,8,11-13] and IRE[17-22] clinical studies, where electrodes were inserted in the vicinity of[3,4,8,11-13,17-22] or into major hepatic vessels.[13] The absence of bleeding, even if needles are inserted deep into the hepatic parenchyma, is an important safety aspect of ECT due to the transient local hypoperfusion and possible electrocoagulation related to the high current density at the surface of needle electrodes.[29,35]

The US findings were dynamic. Hyperechogenic bubbles, which initially form around the electrodes, are a consequence of electrochemical reactions on the electrodes and electrocoagulation of the tissue.[27,29] The liberated gases are chlorine at the anode and hydrogen at the cathode.[42,43] Gas bubbles are formed in RFA[44] and IRE[18,45] ablations. Hypoechogenicity of the treated parenchyma indicates a structural change, which presumably occurs due to decreased perfusion caused by the vasoconstriction and increased wall permeability (edema) of small vessels.[34-37] The histologic findings of the treated hepatic parenchyma immediately after ECT showed fibrin thrombi in small venules, which is consistent with decreased perfusion due to vessel spasms.

Decreased perfusion of the treated areas was confirmed with CEUS and dynamic CT studies, the latter proving the decreased contrast enhancement of the treated areas at 30 to 90 seconds after arterial phase. The area of decreased perfusion was smaller after treatment with fixed hexagonal electrodes than after treatment with variable linear geometry electrodes. This effect is due to a larger distance between electrodes in the case of variable geometry electrodes where higher voltage must be applied to achieve same therapeutic effect, and is in accordance with computer simulation and histology.[28] The difference between the two geometry electrodes can be ascribed to a higher local electric field strength adjacent to the electrodes in the case of linear electrodes[46], as shown in Figure 4A and B. Despite the difference in size of hypoperfused hypoenhancing areas due to the higher local electric field, there is no difference in efficacy of electroporation between the variable linear- and fixed hexagonal-geometry electrodes.[29,46] In routine clinical practice hexagonal electrodes are used for smaller and superficial liver tumors, while linear electrodes are used for deep-seated and larger liver tumors.[47] The subtleness of the radiological changes of liver after EP/ECT agrees with laboratory and histologic findings that the procedure is safe, while on the contrary, it could indicate that CT findings might not be a good indicator of procedure efficacy in healthy liver. The vascular structures of the por-

tal spaces as well as branches of the hepatic and portal veins in the liver parenchyma display different changes depending on their size and position in the ablated area: those situated in the central parts of the ablated areas and close to the electrodes show complete necrosis. Smaller structures are more sensitive to electroporation than larger structures with arterioles and bile canaliculi more resistant than venules.[12]

The CT studies at one week after ECT showed only small hypoenhancing areas, which is in accordance with histologic studies showing the existence of scar tissue.[12,28] Where electrodes punctured the wall of the large vessels, the architecture of the vessel wall was effaced with missing endothelium and no thrombosis present.[28]

Our study has several limitations. Due to the time limit of open surgery, there was limited time for US examinations, and the CT studies were performed in a range of 60 to 90 minutes after the EP/ECT. Performing radiologic examinations at different times was a major limitation because radiologic findings were dynamic and evolved in time. Another limitation of this study is the use of various US machines, which precluded numerical and statistical analyses of the US findings. Different heart rates and blood pressures of pigs influenced CEUS assessment of perfusion; therefore, comparisons among animals would be challenging. Another limitation of the study was that CT studies were only performed at 1 week after ECT with variable linear geometry electrodes. Furthermore, in CT studies, various treated areas could not always be differentiated from other areas. This limitation was overcome in the study with the percutaneous ECT of portal vein tumor thrombosis[13] and in a study with IRE of porcine liver[22] with a coaxial angiocatheter to define electrode orientation and position relative to the ablation zone. Only healthy liver was studied, further investigation of other tissues, particularly tumor tissue is required, because it is reasonable to expect that radiologic findings after ECT of hepatic neoplasia differ from radiologic findings after ECT of healthy liver due to differences in vascular and extracellular spaces. Furthermore, relatively small number of animals has been investigated, which prevented further statistical analyses and a better correlation between different groups.

Conclusions

Radiologic findings after EP/ECT of porcine liver did not show clinically significant damage to large

liver vessels and parenchyma; intact vessel walls and patency were observed, the hepatic parenchymal changes indicated by US hypoechogenicity and CT hypoenhancement were subtle. Histologic changes immediately after, and 2 and 7 days after treatment were in accordance with radiologic findings, and these results confirm that ECT is safe for the treatment of tumors that are adjacent to large hepatic vessels. Notably, radiologic features after EP/ECT are dynamic, and further studies are required to thoroughly investigate these features to provide definite answers, which, if any, are useful as indicators of adequate electric field distribution and as possible predictive factors that could guide decisions regarding the course of further treatment.

Acknowledgements

References

1. Ong SL, Gravante G, Metcalfe MS, Dennison AR. History, ethics, advantages and limitations of experimental models for hepatic ablation. *World J Gastroenterol* 2013; **19:** 147-54. doi: 10.3748/wjg.v19.i2.147

2. Au JT, Kingham TP, Jun K, Haddad D, Gholami S, Mojica K, et al. Irreversible electroporation ablation of the liver can be detected with ultrasound B-mode and elastography. *Surgery* 2013; **153:** 787-93. doi: 10.1016/j.surg.2012.11.022

3. Edhemovic I, Brecelj E, Gasljevic G, Music MM, Gorjup V, Mali B, et al. Intraoperative electrochemotherapy of colorectal liver metastases. *J Surg Oncol* 2014; **110:** 320-7. doi: 10.1002/jso.23625

4. Edhemovic I, Gadzijev EM, Brecelj E, Miklavcic D, Kos B, Zupanic A, et al. Electrochemotherapy: a new technological approach in treatment of metastases in the liver. *Technol Cancer Res Treat* 2011; **10:** 475-85. doi: 10.7785/tcrt.2012.500224

5. Kingham TP, Karkar AM, D'Angelica MI, Allen PJ, DeMatteo RP, Getrajdman GI, et al. Ablation of perivascular hepatic malignant tumors with irreversible electroporation. *J Am Coll Surg* 2012; **215:** 379-87. doi: 10.1016/j.jamcollsurg.2012.04.029

6. Colletti L, Battaglia V, De Simone P, Turturici L, Bartolozzi C, Filipponi F. Safety and feasibility of electrochemotherapy in patients with unresectable colorectal liver metastases: a pilot study. *Int J Surg* 2017; **44:** 26-32. doi: 10.1016/j.ijsu.2017.06.033

7. Tafuto S, von Arx C, De Divitiis, Maura CT, Palaia R, Albino V, et al. Electrochemotherapy as a new approach on pancreatic cancer and on liver metastases. *Int J Surg* 2015; **21:** S78-S82. doi: 10.1016/j.ijsu.2015.04.095

8. Miklavcic D, Mali B, Kos B, Heller R, Sersa G. Electrochemotherapy: from the drawing board into medical practice. *Biomed Eng Online* 2014; **13:** 29. doi: 10.1186/1475-925X-13-29

9. Campana LG, Clover JG, Valpione S, Quaglino P, Gehl J, Kunte C, et al. Recommendations for improving the quality of reporting clinical electrochemotherapy studies based on qualitative systematic review. *Radiol Oncol* 2016; **50:** 1-13. doi: 10.1515/raon-2016-0006

10. Campana LG, Marconato R, Valpione S, Galuppo S, Alaibac M, Rossi CR, et al. Basal cell carcinoma: 10-year experience with electrochemotherapy. *J Transl Med* 2017; **15:** 122. doi: 10.1186/s12967-017-1225-5

11. Djokic M, Cemazar M, Popovic P, Kos B, Dezman R, Bosnjak M, et al. Electrochemotherapy as treatment option for hepatocellular carcinoma, a prospective pilot study. *Eur J Surg Oncol* 2018; **44:** 651-7. doi: 10.1016/j.ejso.2018.01.090

12. Gasljevic G, Edhemovic I, Cemazar M, Brecelj E, Gadzijev EM, Music MM, et al. Histopathological findings in colorectal liver metastasis after electrochemotherapy. *PloS One* 2017; **12:** e0180709. doi: 10.1371/journal.pone.0180709

13. Tarantino L, Busto G, Nasto A, Fristachi R, Cacace L, Talamo M, et al. Percutaneous electrochemotherapy in the treatment of portal vein tumor thrombosis at hepatic hilum in patients with hepatocellular carcinoma in cirrhosis: a feasibility study. *World J Gastroenterol* 2017; **23:** 906-18. doi: 10.3748/wjg.v23.i5.906

14. Granata V, Fusco R, Piccirillo M, Palaia R, Petrillo A, Lastoria S, Izzo F. Electrochemotherapy in locally advanced pancreatic cancer: Preliminary results. *Int J Surg* 2015; **18:** 230-6. doi: 10.1016/j.ijsu.2015.04.055

15. Bimonte S, Leongito M, Granata V, Barbieri A, del Vecchio V, Falco M, et al. Electrochemotherapy in pancreatic adenocarcinoma treatment: preclinical and clinical studies. *Radiol Oncol* 2016; **50:** 14-20. doi: 10.1515/raon-2016-0003

16. Granata V, Fusco R, Setola SV, Palaia R, Albino V, Piccirillo M, et al. Diffusion kurtosis imaging and conventional diffusion weighted imaging to assess electrochemotherapy response in locally advanced pancreatic cancer. *Radiol Oncol* 2019; **53:** 415-24. doi: 10.2478/raon-2019-0004

17. Cannon R, Ellis S, Hayes D, Narayanan G, Martin RCG. Safety and early efficacy of irreversible electroporation for hepatic tumors in proximity to vital structures. *J Surg Oncol* 2013; **107:** 544-9. doi: 10.1002/jso.23280

18. Lee EW, Chen C, Prieto VE, Dry SM, Loh CT, Kee ST. Advanced hepatic ablation technique for creating complete cell death: irreversible electroporation. *Radiology* 2010; **255:** 426-33. doi: 10.1148/radiol.10090337

19. Lee YJ, Lu DS, Osuagwu F, Lassman C. Irreversible electroporation in porcine liver: short- and long-term effect on the hepatic veins and adjacent tissue by CT with pathological correlation. *Invest Radiol* 2012; **47:** 671-5. doi: 10.1097/RLI.0b013e318274b0df

20. Narayanan G, Bhatia S, Echenique A, Suthar R, Barbery K, Yrizarry J. Vessel patency post irreversible electroporation. *Cardiovasc Intervent Radiol* 2014; **37:** 1523-9. doi: 10.1007/s00270-014-0988-9

21. Kasivisvanathan V, Thapar A, Oskrochi Y, Picard J, Leen EL. Irreversible electroporation for focal ablation at the porta hepatis. *Cardiovasc Intervent Radiol* 2012; **35:** 1531-4. doi: 10.1007/s00270-012-0363–7

22. Lee YJ, Lu DS, Osuagwu F, Lassman C. Irreversible electroporation in porcine liver: acute computed tomography appearance of ablation zone with histopathologic correlation. *J Comput Assist Tomogr* 2013; **37:** 154-8. doi: 10.1097/RCT.0b013e31827dbf9b

23. Appelbaum L, Ben-David E, Sosna J, Nissenbaum Y, Goldberg SN. US findings after irreversible electroporation ablation: radiologic-pathologic correlation. *Radiology* 2012; **262:** 117-25. doi: 10.1148/radiol.11110475

24. Abdelsalam ME, Chetta JA, Harmoush S, Ensor J Jr, Javadi S, Dixon K, et al. CT findings after irreversible electroporation ablation in a porcine model: radiologic-pathologic correlation. *J Vasc Interv Radiol* 2013; **24:** S161. doi: 10.1016/j.jvir.2013.01.405

25. Charpentier KP, Wolf F, Noble L, Winn B, Resnick M, Dupuy DE. Irreversible electroporation of the liver and liver hilum in swine. *HPB (Oxford)* 2011; **13:** 168-73. doi: 10.1111/j.1477-2574.2010.00261.x

26. Chung DJ, Sung K, Osuagwu FC, Wu HH, Lassman C, Lu DS. Contrast enhancement patterns after irreversible electroporation: experimental study of CT perfusion correlated to histopathology in healthy porcine liver. *J Vasc Interv Radiol* 2016; **27:** 104-11. doi: 10.1016/j.jvir.2015.09.005

27. Boc N, Edhemovic I, Kos B, Music MM, Brecelj E, Trotovsek B, et al. Ultrasonographic changes in the liver tumors as indicators of adequate tumor coverage with electric field for effective electrochemotherapy. *Radiol Oncol* 2018; **52:** 383-91. doi: 10.2478/raon-2018-0041

28. Zmuc J, Gasljevic G, Sersa G, Edhemovic I, Boc N, Seliskar A, et al. Large liver blood vessels and bile ducts are not damaged by electrochemotherapy with bleomycin in pigs. *Sci Rep* 2019; **9:** 3649. doi: 10.1038/s41598-019-40395-y

29. Kos B, Voigt P, Miklavcic D, Moche M. Careful treatment planning enables safe ablation of liver tumors adjacent to major blood vessels by percutaneous irreversible electroporation (IRE). *Radiol Oncol* 2015; **49:** 234-41. doi: 10.1515/raon-2015-0031

30. Marčan M, Pavliha D, Kos B, Forjanič T, Miklavčič D. Web-based tool for visualization of electric field distribution in deep-seated body structures and planning of electroporation-based treatments. *Biomed Eng Online* 2015; **14 Suppl 3:** S4. doi: 10.1186/1475-925X-14-S3-S4

31. Marty M, Sersa G, Rémi Garbay J, Gehl J, Collins CG, Snoj M, et al. Electrochemotherapy – an easy, highly effective and safe treatment of cutaneous and subcutaneous metastases: results of ESOPE (European Standard Operating Procedures of Electrochemotherapy) study. *EJC Supplements* 2006; **4:** 3-13. doi: 10.1016/j.ejcsup.2006.08.002

32. Mir LM, Gehl J, Sersa G, Collins CG, Garbay JR, Billard V, et al. Standard operating procedures of the electrochemotherapy: instructions for the use of bleomycin or cisplatin administered either systemically or locally and electric pulses delivered by Cliniporator by means of invasive or non-invasive electrodes. *Eur J Cancer Suppl* 2006; **4:** 14-25. doi: 10.1016/j.ejcsup.2006.08.003

33. Nykonenko A, Vavra P, Zonca P. Anatomic peculiarities of pig and human liver. *Exp Clin Transplant* 2017; **15:** 21-6. doi: 10.6002/ect.2016.0099

34. Bellard E, Markelc B, Pelofy S, Le Guerroué, Sersa G, et al. Intravital microscopy at the single vessel level brings new insights of vascular modification mechanisms induced by electropermeabilization. *J Control Release* 2012; **163:** 396-403. doi: 10.1016/j.jconrel.2012.09.010

35. Jarm T, Cemazar M, Miklavcic D, Sersa G. Antivascular effects of electrochemotherapy: implications in treatment of bleeding metastases. *Expert Rev Anticancer Ther* 2010; **10:** 729-46. doi: 10.1586/era.10.43

36. Gehl J, Skovsgaard T, Mir LM. Vascular reactions to in vivo electroporation: characterization and consequences for drug and gene delivery. *Biochim Biophys Acta* 2002; **1569:** 51-8. doi: 10.1016/s0304-4165(01)00233-1

37. Markelc B, Bellard E, Sersa G, Jesenko T, Pelofy S, Teissié, et al. Increased permeability of blood vessels after reversible electroporation is facilitated by alterations in endothelial cell-to-cell junctions. *J Control Release* 2018; **276:** 30-41. doi: 10.1016/j.jconrel.2018.02.032

38. Ivanusa T, Beravs K, Cemazar M, Jevtic V, Demsar F, Sersa G. MRI macromolecular contrast agents as indicators of changed tumor blood flow. *Radiol Oncol* 2001; **35:** 139-47.

39. Sersa G, Cemazar M, Miklavcic D. Tumor blood flow modifying effects of electrochemotherapy: a potential vascular targeted mechanism. *Radiol Oncol* 2003; **37:** 43-8.

40. Sersa G, Cemazar M, Miklavcic D, Chaplin DJ. Tumor blood flow modifying effect of electrochemotherapy with bleomycin. *Anticancer Res* 1999; **19:** 4017-22.

41. Sersa G, Cemazar M, Parkins CS, Chaplin DJ. Tumour blood flow changes induced by application of electric pulses. *Eur J Cancer* 1999; **35:** 672-7. doi: 10.1016/s0959-8049(98)00426-2

42. Li K, Xin Y, Gu Y, Xu B, Fan D, Ni B. Effects of direct current on dog liver: possible mechanisms for tumor electrochemical treatment. *Bioelectromagnetics* 1997; **18:** 2-7. doi: 10.1002/(sici)1521-186x(1997)18:1<2::aid-bem2>3.0.co;2-6

43. Stehling MK, Guenther E, Mikus P, Klein N, Rubinsky L, Rubinsky B. Synergistic combination of electrolysis and electroporation for tissue ablation. *PloS One* 2016; **11:** e0148317. doi: 10.1371/journal.pone.0148317

44. Oei T, vanSonnenberg E, Shankar S, Morrison PR, Tuncali K, Silverman SG. Radiofrequency ablation of liver tumors: a new cause of benign portal venous gas. *Radiology* 2005; **237:** 709-17. doi: 10.1148/radiol.2372041295

45. Faroja M, Ahmed M, Appelbaum L, Ben-David E, Moussa M, Sosna J. Irreversible electroporation ablation: is all the damage non thermal? *Radiology* 2013; **266:** 462-70. doi: 10.1148/radiol.12120609

46. Miklavcic D, Semrov D, Mekid H, Mir LM. A validated model of in vivo electric field distribution in tissues for electrochemotherapy and for DNA electrotransfer for gene therapy. *Biochim Biophys Acta* 2000; **1523:** 73-83. doi: 10.1016/s0304-4165(00)00101-x

47. Miklavcic D, Sersa G, Brecelj E, Gehl J, Soden D, Bianchi G, et al. Electrochemotherapy: technological advancements for efficient electroporation-based treatment of internal tumors. *Med Biol Eng Comput* 2012; **50:** 1213-25. doi: 10.1007/s11517-012-0991-8